eTransportation 22 (2024) 100370

Contents lists available at ScienceDirect

eTransportation

journal homepage: www.journals.elsevier.com/etransportation

Microstructure-based digital twin thermo-electrochemical modeling of LIBs at the cell-to-module scale

Siyoung Park [a], Hyobin Lee [a], Seungyeop Choi [a,b], Jaejin Lim [a,b], Suhwan Kim [a], Jihun Song [a], Mukarram Ali [c,d], Tae-Soon Kwon [e,***], Chilhoon Doh [c,d,**], Yong Min Lee [a,b,*]

[a] Department of Energy Science and Engineering, Daegu Gyeongbuk Institute of Science and Technology (DGIST), Daegu, 42988, Republic of Korea
[b] Department of Chemical and Biomolecular Engineering, Yonsei University, Seoul, 03722, Republic of Korea
[c] Next Generation Battery Research Center, Korea Electrotechnology Research Institute (KERI), Changwon, 51543, Republic of Korea
[d] Department of Electric Energy Materials Engineering, University of Science and Technology (UST), Changwon, 51543, Republic of Korea
[e] Railroad Safety Research Division, Korea Railroad Research Institute (KRRI), Uiwang, 16105, Republic of Korea

ARTICLE INFO

Keywords:
Thermal analysis
Digital twin
Microstructure-based model
Railway vehicle
Li-ion battery
Safety

ABSTRACT

As the application of lithium-ion batteries (LIBs) expands beyond conventional electric vehicles (EVs) to heavy vehicles such as electric trucks or trams, the importance of thermal management in LIB systems is increasing, even at the module or pack level. In particular, because monitoring the thermal behaviors of each cell is not feasible, thermo-electrochemical modeling and simulations in the module or pack level are essential for analyzing and ensuring thermal stability. However, because the conventional lumped thermo-electrochemical models cannot reflect the actual structure of LIB cells, there might be considerable differences may exist between simulation and experimental results. To fill these gaps, we have newly developed a 3D microstructure-based digital twin model of a battery module (8.8 Ah/18.5 V, five LIB pouch cells in series) for an unmanned railway vehicle. Unlike traditional lumped models, our digital twin model accurately well reflects the internal structure of cells and can calculate the heat generation of each component inside a cell. As a result, contrary to a lumped model, the digital twin model can not only simulate the inhomogeneous temperature gradient inside a cell, but also estimates higher local maximum temperatures ($T_{DT,\ max}/T_{L,\ max}$ = 137.2 °C/123.9 °C @ 10C discharge) in cells which can trigger thermal runaway. Therefore, microstructure-based digital twin modeling can alleviate concerns regarding the thermal runaway of LIB cells, modules, and packs, and provide safe operating conditions.

1. Introduction

Owing to the high energy density and affordable cost of lithium-ion batteries (LIBs), their usage has expanded to heavy transportation systems such as electric buses and trucks [1]. Moreover, considerable efforts have been made to utilize LIBs in railway transportation such as trams and light railway vehicles [2,3]. However, as both the energy density and capacity of LIB cells have increased, their thermal behavior has attracted increasing attention for long-term fire- or explosion-free operations [4,5]. In particular, when multiple cells are loaded in series or parallel at the module or pack level, thermal management becomes more difficult and even challenging depending on the number of LIB cells. Hence, we must address the risk of thermal propagation of one abnormal cell towards neighboring normal cells [6–8]. In this regard, the overall temperatures above the module level are monitored using limited thermocouples and controlled by cooling or heating systems under battery management systems [9–12]. However, with limited thermocouples that measure only the surface temperatures of certain cells, the local maximum temperatures, which trigger the thermal runaway (TR) of a cell, cannot be accurately estimated or properly controlled under safe operating conditions through appropriate management.

To solve this practical problem, many previous studies have already used simple battery models and simulations to monitor and predict the

* Corresponding author. Department of Chemical and Biomolecular Engineering, Yonsei University, Seoul, 03722, Republic of Korea.
** Corresponding author. Next Generation Battery Research Center, Korea Electrotechnology Research Institute (KERI), Changwon, 51543, Republic of Korea.
*** Corresponding author. Railroad Safety Research Division, Korea Railroad Research Institute (KRRI), Uiwang, 16105, Republic of Korea.
E-mail addresses: klez@krri.re.kr (T.-S. Kwon), chdoh@keri.re.kr (C. Doh), yongmin@yonsei.ac.kr (Y.M. Lee).

https://doi.org/10.1016/j.etran.2024.100370
Received 12 August 2024; Received in revised form 26 September 2024; Accepted 12 October 2024
Available online 16 October 2024

thermal behavior across an entire LIB cell, module, or pack systems [13–19], equivalent circuit models [20–25], and physics-based electrochemical models [26–32]. However, to shorten the calculation time using minimal memory resources, most of these models have been coupled with thermal models in a lumped structure, which cannot reflect the actual internal structure of LIB cells. However, conventional lumped models have shown limitations in predicting maximum temperatures within a cell, especially under harsh operating conditions such as high operating temperatures [33–35]. Extreme conditions (e.g., high charge/discharge rates and extremely high external temperatures) can cause extreme thermal behavior owing to the internal design of a system; therefore, a more precise simulation method is required. For this reason, the inner structures of LIB cells have been more carefully built to simulate thermal behaviors more reliably [36–40]. Microstructure-based models can not only accurately predict maximum temperatures inside a cell, which can result in the TR of the cell caused by an internal short-circuit (ISC) [29,41,42], but can also investigate the effect of cell design parameters (e.g., electrode thickness, current collector thickness, lead tab size, thickness, and locations) on the thermal behavior of a cell. Furthermore, as the cell design becomes more severe, microstructure-based models have been extensively developed despite their increased memory resources and longer computation times, which have limited their applications at the single-cell level. However, because LIB modules/packs with multiple cells are used in various applications, it is essential to expand this microstructure-based cell model into modules or packs to reflect the additional heating caused by neighboring cells and module/pack structures.

For this purpose, we built a microstructure-based digital twin model that reflects the detailed structure inside cells at both cell and module levels. We then coupled three types of computational physics (electrochemistry in P2D, current distribution in 3D, and thermal behavior in 3D), which together provided feedback in real-time [43,44]. In addition, to achieve high reliability in our model, we disassembled 8.8 Ah pouch LIB cells to maintain the internal structural design and electrochemical parameters [30,45]. Besides the simulation, we designed, fabricated, and evaluated an 18.5 V/8.8 Ah module using five pouch cells in series, which was developed as a power source for unmanned railway vehicles especially for fire accidents in tunnels or undergrounds. Both experiments and simulations were conducted at room temperature (25 °C) under various discharge rates (0.1, 0.5, 1, 3, and 5C) for their electrochemical and thermal behaviors. Moreover, to compare and emphasize the necessity of our digital twin model, we additionally built a conventional lumped model at the module scale, where the cell structure was reflected only as a box. Finally, from a practical perspective, we simulated electrochemical and thermal behavior by applying two types of railway current patterns (Mikuni and Katsuyama patterns) to the module.

2. Experimental section

2.1. Thermo-electrochemical evaluation of cell and module

We utilized 8.8 Ah pouch-type commercial cells using $LiNi_{0.4}Co_{0.3}Mn_{0.3}O_2$ (NCM) and graphite as active materials (Fig. S1). These cells were used to fabricate a power source module for an unmanned railway vehicle (Fig. S2). Because this vehicle was designed to operate in unelectrified and fire situations in tunnels or underground, the module case was composed of polyetheretherketone (PEEK), which has high thermal stability and strong mechanical strength over a wide temperature range. To satisfy the requirements such as power and operating time, five cells were connected in series (nominal capacity/voltage: 8.8 Ah/18.5 V). To evaluate both electrochemical and thermal behaviors simultaneously, a cycler of 300 A/5 V (PEBC05-300, PNE) was used for the unit cell, and another cycler of 60 A/48 V (BNT60-048-5 ME, Digatron) was used for the module (Fig. S3). Both the cell and module were charged using these cyclers in CC/CV mode at 0.5C (cut-off condition: 0.05C; 0.44 A), while discharging was performed in CC mode at each C-rate (cut-off condition: 3.0 V). For the module test, which involved a much higher current flow than the unit cell, thick cables were used, and the tabs and jigs were welded to reduce the IR drop. Thermocouples were attached to the cell (one point at the front surface) and the module (three points: top, side, and bottom) to measure the temperature changes under different discharge rates (0.1, 0.5, 1, 3, and 5C) at a constant room temperature of 25 °C. The accuracy of the simulation compared to the experiment was calculated using Root Mean Square Error (RMSE) as shown in the following equation (1):

$$RMSE = \sqrt{\sum_{i=1}^{N} \frac{(Simulation - Experiment)^2}{N}} \quad (1)$$

where N is the number of data. Finally, two railway driving patterns were applied to the module in the commercial perspective. The LIBs in the railcar from previous literature was replaced by the module developed in this study, the discharge current applied to the module was converted based on the same C-rate [40].

2.2. Thermal behavior evaluation

Differential scanning calorimetry (DSC; Discovery DSC, TA Instruments) was used to determine the melting temperature of the separator. After cell disassembly, the separators were dried in a vacuum oven at 50 °C for 12 h to prepare the samples. The DSC measurement temperature range was 25–150 °C, with a heating rate of 5 °C min^{-1} under flowing N_2 gas. An accelerating rate calorimetry (ARC, Fig. S4) experiment was conducted using extended volume–ARC (EV–ARC; EV+ Accelerating Rate Calorimeter, Thermal Hazard Technology) to determine the critical temperature required to reach the self-heating stage (SHS). Before the critical temperature, the ARC caused a step-wise increase in the temperature of the chamber by 5 °C, which was maintained for 1 h, after which until the temperature sensitivity rate exceeded 0.02 °C min^{-1}, this operation mode is known as heat-wait-seek (HWS). Beyond the SHS, as the cell temperature rises continuously, it eventually reaches the ignition point, leading to TR stage (TRS). The maximum temperature and voltage were also measured during this process.

2.3. Parameter mining and numerical method

To build a reliable model, structural and electrochemical parameters were chosen by disassembling the commercial pouch cell in a dry room (dew point under −60 °C, Fig. S5). The internal structural parameters (e.g., length, width, and thickness) were directly measured, and a 2032 half-cell with a cathode or anode was fabricated to determine the electrochemical parameters (Fig. S6). In more detail, the cathode and anode sheets were immediately washed using dimethyl carbonate (DMC) after disassembly and then dried in a vacuum oven at 60 °C for 12 h. As the electrodes were double side coated, one side was removed using *N*-methyl-2-pyrrolidone (NMP) for the cathode, and H_2O for the anode. The electrodes were punched into circles with a 12 mm diameter, while the counter lithium metal had a 16 mm diameter (thickness = 200 μm). Additionally, a polyethylene (PE) separator (diameter = 18 μm, T20BHE, Tonen, Japan) and 100 μL of electrolyte (1.15M $LiPF_6$ in EC/EMC (3/7, v/v), Enchem, Korea)) were used. The voltage range of the cathode half-cell was 3.0–4.3 V vs. Li/Li^+, and that of the anode was 0.005–1.5 V vs. Li/Li^+. Using these half-cells, equilibrium potentials were measured at a 0.01C (Figs. S6b and c), and the diffusion coefficient and exchange current density were measured using the galvanostatic intermittent titration technique method. Based on these parameters, our microstructure-based digital twin model was built using COMSOL Multiphysics 6.2 (COMSOL Inc., USA), coupled with P2D electrochemical, 3D thermal, and 3D current distribution physics (Table S2). The simulations were performed using an AMD Ryzen Threadripper PRO

5995WX central processing unit with 1 TB of memory. The thermal behavior was also calculated as following energy conversion equation (2):

$$mC_p\frac{dT}{dt} = Q_{gen} - Q_{conv} = Q_{gen} - hA(T - T_A) \quad (2)$$

Where m is mass, C_p is the heat capacity, T is the temperature of the cell, h is the heat transfer coefficient, A is total surface area of heat dissipation, and T_A is external ambient temperature. The accumulated heat inside the cell can be expressed by the difference between the heat generation (Q_{gen}) and heat dissipation by convection (Q_{conv}). However, the total heat generation in this model consisted of reversible (entropic change) and irreversible (joule heating) terms, based on the thermodynamic energy balance [46]. In this model, the heat generation was calculated from P2D electrochemical, and 3D current distribution physics which were simultaneously coupled with the 3D thermal model in a time-dependent simulation (Table S3). The heat source can be demonstrated simply as follows Equation (3):

$$Q_{gen} = I(U_{OCP} - V) + IT\frac{dU_{OCP}}{dT} = I^2R + IT\frac{dU_{OCP}}{dT} \quad (3)$$

where q is the heating rate, I is the current, R is the resistance, V is operating voltage and U_{OCP} is the open-circuit potential of the battery. The heat sources from t were calculated depending on the discharge capacity (Fig. S7). Symbols and governing equations are listed in Tables S1 and S2. To simulate the heat flux physics more accurately, heat dissipation from the surface of the cell and module was calculated using natural convection physics (conditions similar to the experimental setup inside the chamber), with the heat transfer coefficient (HTC) adjusted by comparing the experimental results at a 0.1C discharge rate (h = 10–15 W m^{-2} K^{-1}).

3. Results and discussion

For a systematic investigation of thermal analysis through microstructure-based digital twin modeling, we validated the electrochemical and thermal behaviors before expanding the simulation of the module level. Since cell surface temperatures can be measured directly using thermocouples (Fig. 1a), an evaluation at the cell level was required to validate the thermal behaviors. The model incorporated internal structures including tabs, separators, and electrodes, which enabled the simulation of the heat generation and propagation, based on the cell's internal design (Fig. 1b).

Using this microstructure-based model, we simulated heat generation, transfer, and dissipation in real-time using the finite element method (FEM). Heat generation, including entropic heat (electrochemical reaction heat and reversible heat), was evaluated using P2D electrochemical physics, while Joule heat (Ohmic heat, and irreversible heat) due to current flow was calculated using 3D current distribution physics (Fig. 1c). These heat sources were applied in 3D thermal physics. As the temperature of the cell increased due to the presence of these heat sources, heat dissipation via natural convection occurred on the surface of the cell. The temperature of each domain was fed back into the electrochemical and current distribution models, updating the heat sources according to the temperature in each domain. The equilibrium potential was included in the electrochemical evaluation of the cathode and anode half-cells. The diffusion coefficient and exchange current density values were also applied as functions of the state of lithiation and temperature (Table S4). Heat dissipation from the battery surface was calculated using internal natural convection physics, with the HTC adjusted based on temperature results from a 1C discharge rate. The HTC value was calculated to range from 10 to 15 W m^{-2} K^{-1}.

Fig. 2 shows a comparison between the experimental and simulation results obtained under various discharge rates (0.1, 0.5, 1, 3, and 5C), based on this digital twin model at the cell level. The results of the cell-

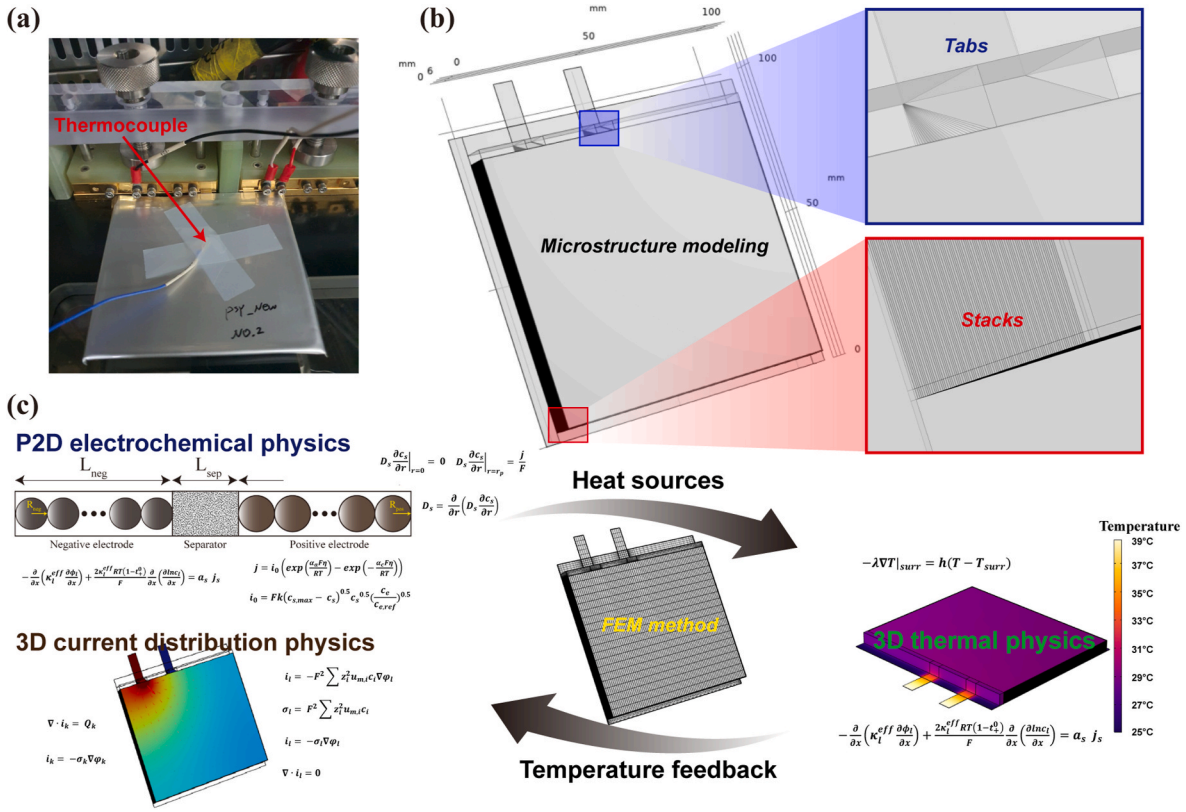

Fig. 1. Overall design of experiment and simulation. (a) Cell image attached with thermocouple inside the chamber. (b) Microstructure-based digital twin structure image. (c) Physics and method of simulation: Coupling P2D electrochemical, 3D current distribution, and 3D thermal physics.

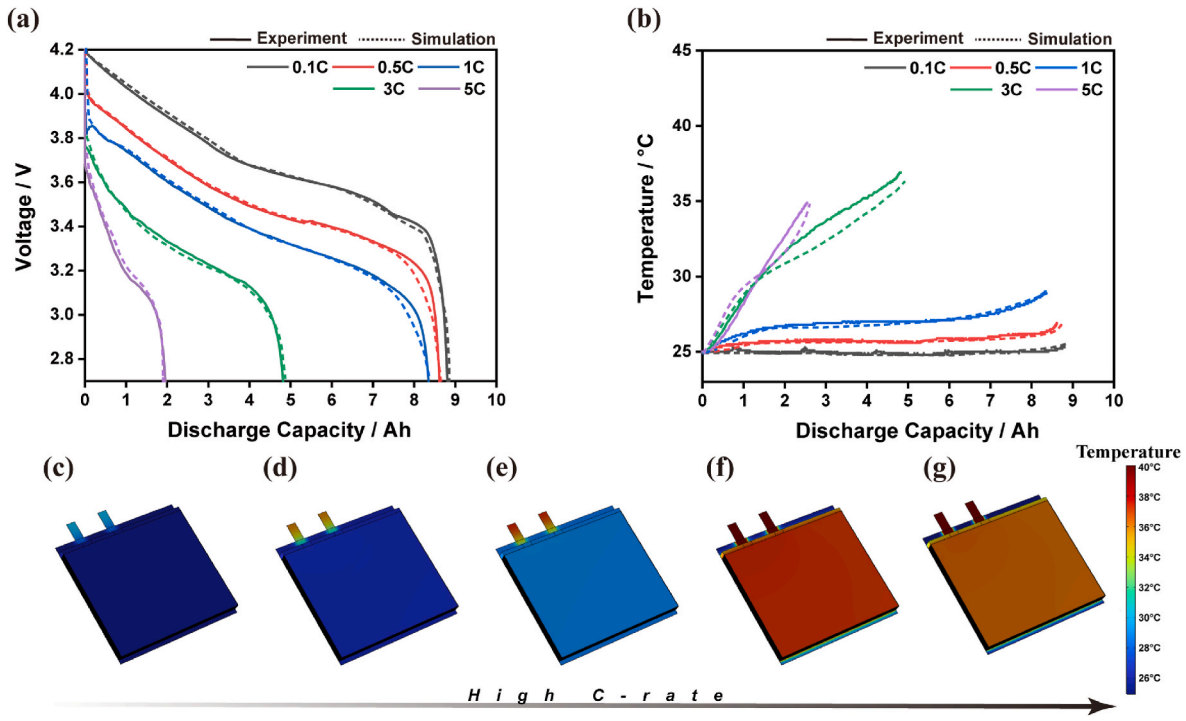

Fig. 2. Experimental and simulation results of unit cell. (a) Voltage profiles, and (b) surface temperature profiles. (c–g) 3D temperature images at different discharge rates: (c) 0.1C, (d) 0.5C, (e) 1C, (f) 3C, and (g) 5C.

level modeling (Fig. 2a and b) reveal high consistency of maximum temperature (RMSE values under 1) between the experimental and simulated electrochemical and thermal behaviors, indicating the high reliability of our model (Table S5). The 3D temperature distribution of the unit cell under different discharge rates shown in Fig. 2c–g and the heat source per volume graph was shown in Fig. S7a. As expected, higher discharge rates resulted in greater temperature increases and showed significant higher heat generation rate per time than lower rates. However, notably, the temperature curves under 3C and 5C discharge rates show reversed trends. Although the heat generation per hour was higher at 5C than 3C, the shorter discharge time at 5C resulted in lower total heat generation compared to 3C.

Based on a digital twin model verified at the cell level, we expanded our model to the module scale. This module was designed as a power source for unmanned railway vehicles (Fig. S2). Since the vehicle was designed to operate in fire situations, the module case was composed of PEEK, a material known for its high thermal stability and strong mechanical properties. To achieve the required power for the unmanned railway vehicle, five 8.8 Ah cells were connected in series (Fig. 3a and b). We built a digital twin model that reflected the internal structure of each cell and its connections (Fig. 3c). Similar to previous cell modeling methods, the module scale modeling included a P2D electrochemical model, 3D current distribution, and 3D thermal physics. However, owing to the complexity of the structure and incorporation of various physical phenomena, the modeling process became more challenging and required remarkably longer computation time than compared to conventional lumped models. Nonetheless, this detailed model allows for accurate measurement of maximum internal temperature, making it suitable for considering melting of the separators and ISCs, which are major causes of TR.

Using the microstructure-based digital twin model at the module scale, Fig. 4 illustrates the experimental and simulation results through voltage and temperature curves. Fig. 4a shows the experimental temperature curves of the module during the entire cycling process, displaying the temperature changes on the surface of the three different regions (top, bottom, and side) of the module. Our simulation results match the experimental results with high reliability (Fig. 4b and c, Table S6), depicting the 3D surface temperature gradient of the module (Fig. 4d–h).

An interesting observation was made from the maximum temperature values at the five different discharge rates (Table 1), as shown in Fig. 4a. At discharge rates below 1C, the temperature of the bottom

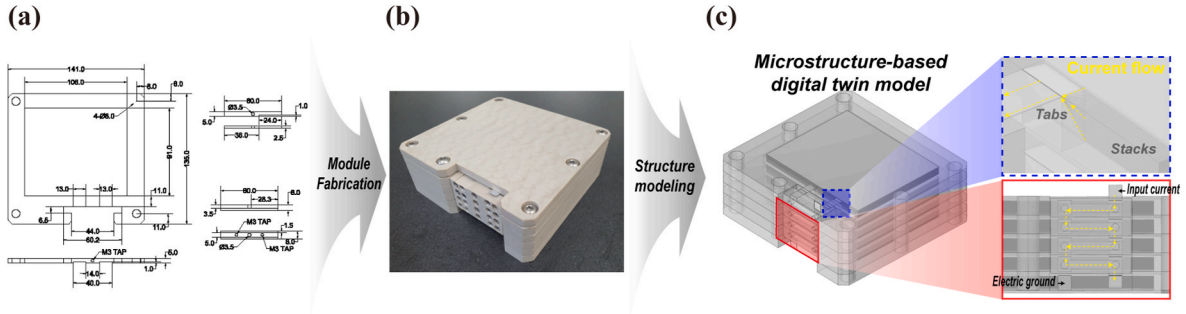

Fig. 3. Module design, fabrication and digital twin structure. (a) Structural drawing of module. (b) Actual module image. (c) Microstructure-based digital twin model for simulation.

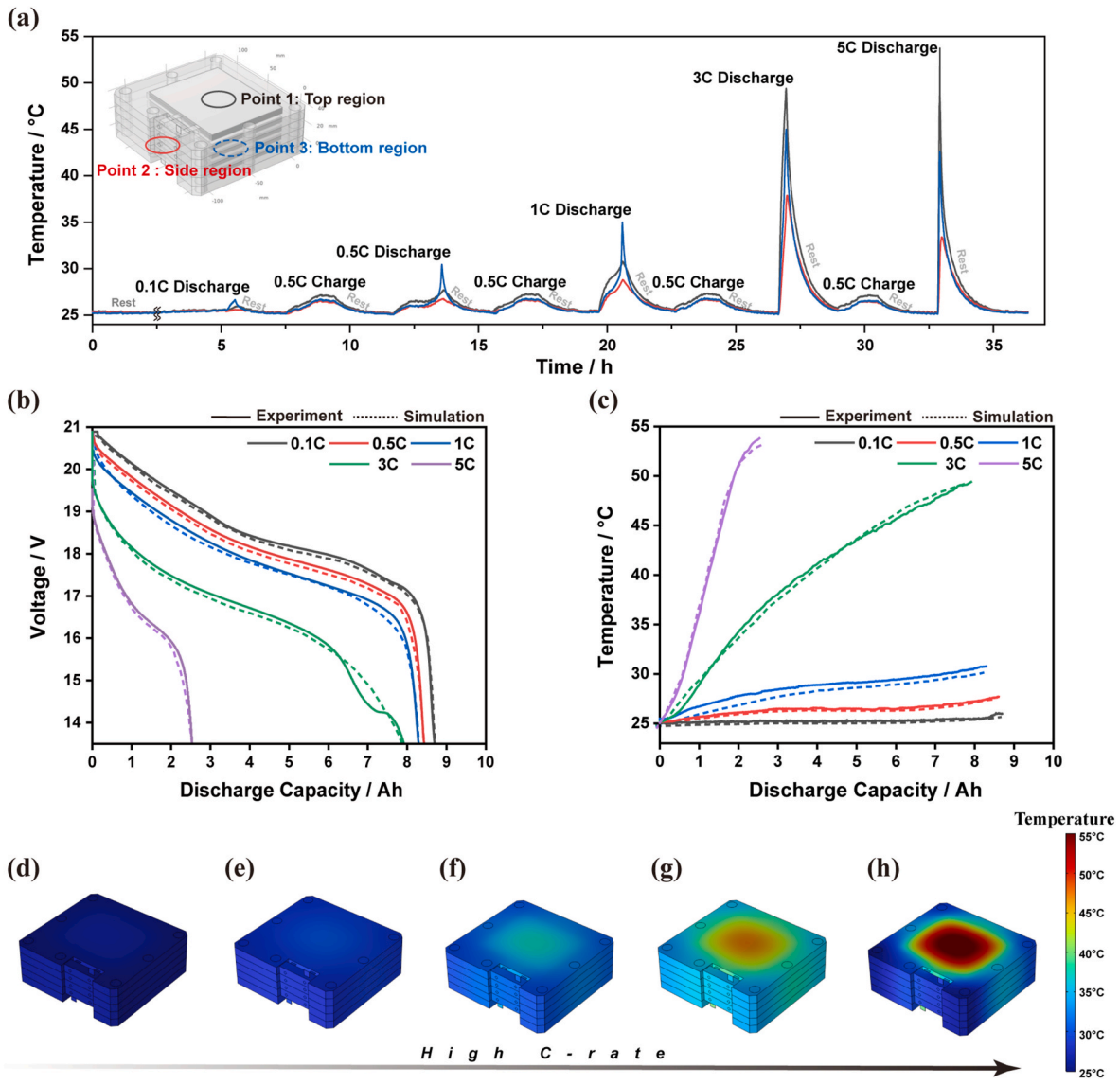

Fig. 4. Experimental and simulation results of module. (a) Experimental results: temperature curves of three different regions during cycling. Experiment and simulation comparisons of (b) discharge voltage, and (c) top surface temperature. (d–h) 3D temperature distribution of module surface depending on different discharge rates: (d) 0.1C, (e) 0.5C, (f) 1C, (g) 3C, and (h) 5C.

Table 1
Experimental results: maximum temperature of three different regions depending on discharge rates.

Regions	0.1C	0.5C	1C	3C	5C
Top region (black line)	25.9°C	27.7°C	30.7°C	49.4°C	53.7°C
Bottom region (blue line)	26.6°C	30.4°C	35.0°C	44.9°C	42.6°C
Side region (red line)	25.6°C	26.7°C	28.8°C	37.9°C	33.4°C

region (blue line) was the highest, but above 3C, the top region showed the highest temperature. This was because the top case was designed to be thinner than the bottom case. It is important to note that the thermal conductivity of PEEK is low (0.29 W m^{-1} K^{-1} @ 25 °C), making it difficult to dissipate heat quickly through natural convection, leading to heat accumulation in the module. Especially under the 5C discharge condition, the heat generation rate per hour is more than 10 times higher than at 1C, causing a rapid temperature rise. In this sense, at high discharge rates of over 3C, the temperature of the thin top region increased more quickly at the beginning of discharge. In contrast, at discharge rates below 1C, which provided more time for heat accumulation, the temperature of the bottom region gets increased. Interestingly, at low discharge rates below 1C, the temperature of the top region was initially (at the beginning of discharge) higher than that of the bottom region. This indicates that the top region's temperature changed quickly due to the thinner PEEK case.

For safety reasons, at discharge rates up to 5C, we conducted only thermal simulations, without experiments. Fig. 5 shows the temperature distribution of the cross-sectional view under a 10C discharge condition. To demonstrate the superiority of our microstructure-based digital twin model, we created a conventional lumped model and compared their thermal behaviors. In the lumped model, the cell structure was represented as a simple box that does not reflect the internal structure of a cell, with only thermo-electrochemical physics coupling. The heat source from the P2D electrochemical model was uniformly applied to the box-type cells, in units of watts per volume. Besides, the anisotropic thermal conductivity of the lumped model was employed for both in-plane and through-plane directions [47,48]. To ensure a reasonable comparison between the two models, the surface temperatures of the module (top region) were set to be the same. As shown in Fig. 5b, the lumped model exhibited homogeneous heat conduction and a uniform

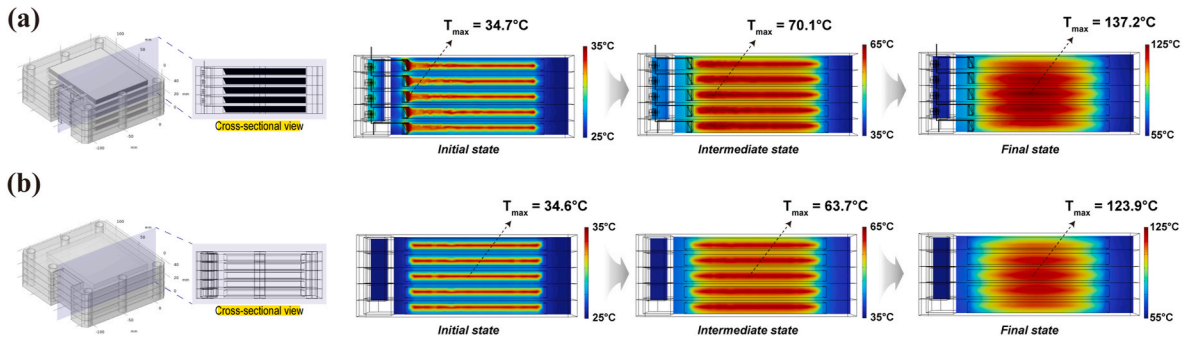

Fig. 5. Comparison of a digital twin model with a lumped model. Structural image, and temperature gradient of cross-sectional view depending on discharge process: (a) Digital twin model, and (b) lumped model.

temperature distribution inside the cell, with the maximum temperature consistently located in the middle of the innermost cell. In contrast, the digital twin model showed an inhomogeneous temperature gradient depending on the discharge time, because it could correctly calculate the internal heat generation by reflecting the internal structure of the cell. (Fig. 5a). At the beginning of the discharge process, the highest temperature within the module was located near the tabs inside the center cell. As the discharge progressed, the temperature distribution inside the cell exhibited a trend similar to that of the lumped model. Since the maximum temperature inside the module depended only on heat generation; however, over time, the effect of heat dissipation from the surface of the module became more significant. At the end of the discharge, the difference in maximum temperature between the digital twin model and the lumped model was considerable ($T_{DT,\ max}/T_{L,\ max}$ = 137.2 °C/123.9 °C). Unlike the lumped model, which applies the total heat generation per cell volume uniformly (from only P2D electrochemical model), the digital twin model accounts for the heat generation of each internal structure within a cell (from P2D electrochemical and 3D current distribution model), although the total heat generation of the cells was almost same. This difference was particularly pronounced at a high discharge rate of 10C, where the maximum temperature differences became more evident. Consequently, creating a reliable model without considering the structural influences within a cell would be difficult. This omission from the conventional modeling method can lead to significant error, particularly at high discharge rates, which cause massive heat generation per unit time. Fig. S8 shows the thermal stability of the unit cell of our module system, based on the ARC and DSC analysis results. In the ARC results, the initial voltage drop

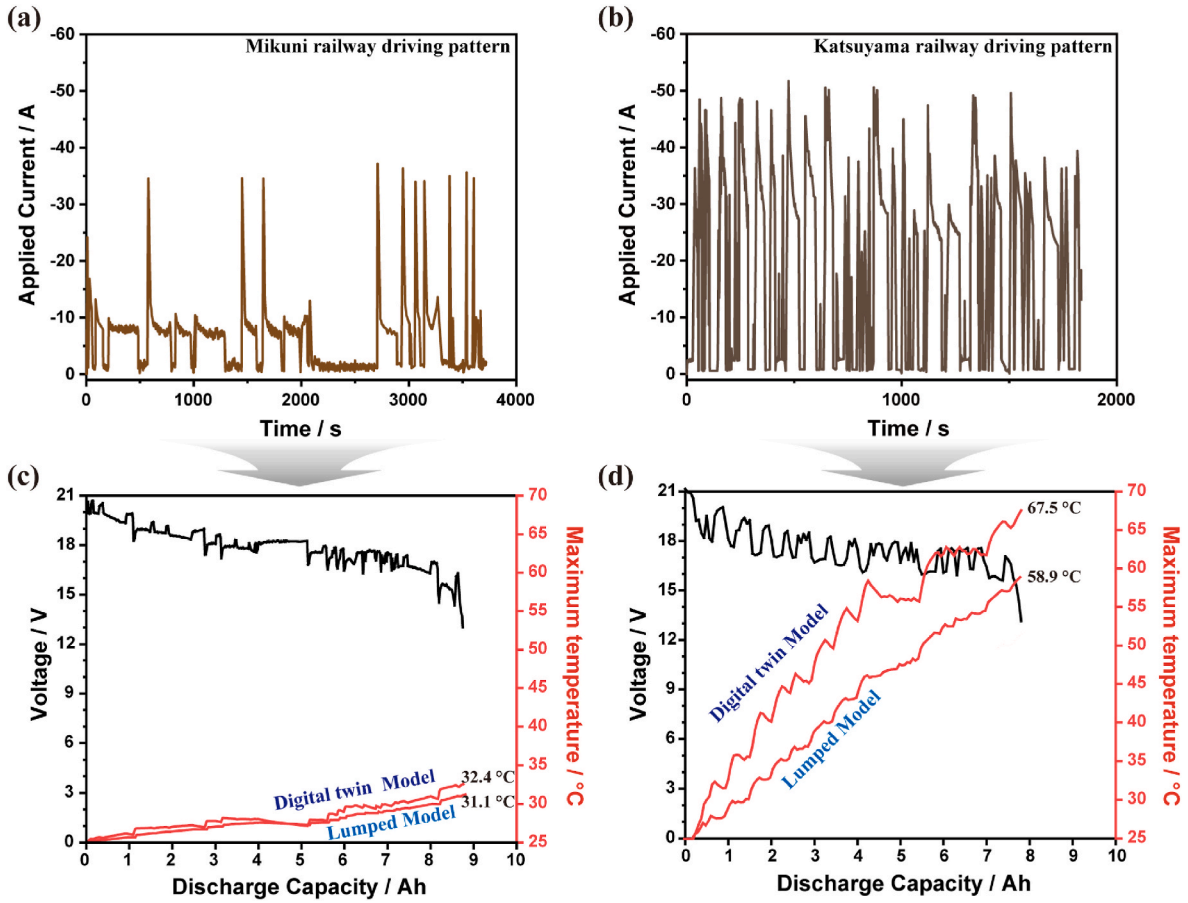

Fig. 6. Simulation results obtained by applying two types of railway driving patterns. Applied discharge current of (a) Mikuni railway pattern, and (b) Katsuyama railway pattern. Voltage and maximum temperature curves of digital twin model and lumped model: (c) Mikuni pattern, and (d) Katsuyama pattern.

began at 132 °C due to separator melting, followed by self-heating until TR was reached (Fig. S8a). Similarly, in the DSC results, melting of the separator was observed at approximately 120–130 °C. Since the conventional lumped model cannot predict maximum temperatures above 120 °C inside a module, it is evident that it may fail to accurately predict TR, whereas the digital twin model can provide reliable TR predictions in advance.

Finally, from a practical perspective, the proposed model was evaluated by applying two types of railway vehicle driving patterns (Fig. 6). The discharge current for each pattern was calculated according to the specifications of our module, based on the discharge rate of a single cell in the railway vehicle. In the Mikuni pattern, there is one rest period around 2000–3000 s, and the discharge current did not fluctuate significantly compared to the Katsuyama pattern (Fig. 6a and b). As depicted in Fig. 6c and d, the Mikuni pattern showed a low maximum temperature difference of 1.3 °C ($T_{DT,\ max}/T_{L,\ max}$ = 32.4 °C/31.1 °C), while the Katsuyama pattern exhibited a maximum temperature difference of 8.6 °C ($T_{DT,\ max}/T_{L,\ max}$ = 67.5 °C/58.9 °C). Therefore, our microstructure-based digital twin model provides more accurate predictions of maximum temperature, contributing to prevention of reaching dangerous temperature at module level. Furthermore, we anticipate that our model will enable more detailed thermal evaluations under abnormal or extreme conditions, making it an effective tool for preventing TR.

4. Conclusion

We successfully developed a microstructure-based digital twin battery model that reflects the internal structure of a cell, and the parameters measured from disassembled pouch cells. Our digital twin model could adequately simulate both the electrochemical and thermal behaviors of a battery module (8.8 Ah/18.5 V, five cells in series) with a high accuracy in voltage profiles even under various discharge rates (0.1, 0.5, 1, 3, and 5C). When this model was compared with a conventional lumped model under extreme conditions such as 10C discharge, a higher maximum temperature ($T_{DT,\ max}/T_{L,\ max}$ = 137.2 °C/123.9 °C) was simulated in the digital twin model, which implied that lumped models may not predict TR situation. In other words, without reflecting the internal structure of cells, the catastrophic thermal behavior of modules cannot be estimated using lumped models. Additionally, since the module was originally designed as a power source for unmanned railway vehicles, we tested our model with two different railway driving patterns as a practical perspective. Our digital twin model predicted higher maximum temperatures than a lumped model, emphasizing the importance of incorporating the detailed internal structure of cells into models. This study lays the foundation for future research in optimizing battery thermal management and ensuring safety in advanced energy storage systems.

CRediT authorship contribution statement

Siyoung Park: Writing – review & editing, Writing – original draft, Visualization, Validation, Software, Methodology, Conceptualization. **Hyobin Lee:** Resources, Methodology. **Seungyeop Choi:** Validation, Investigation. **Jaejin Lim:** Methodology, Data curation. **Suhwan Kim:** Validation, Methodology. **Jihun Song:** Resources, Methodology. **Mukarram Ali:** Resources. **Tae-Soon Kwon:** Resources, Project administration, Methodology. **Chilhoon Doh:** Resources, Methodology, Data curation, Conceptualization. **Yong Min Lee:** Writing – review & editing, Writing – original draft, Supervision, Project administration, Methodology, Conceptualization.

Declaration of competing interest

The authors declare that they have no known competing financial interests or personal relationships that could have appeared to influence the work reported in this paper.

Acknowledgement

This work is supported by the Korea Agency for Infrastructure Technology Advancement (KAIA) grant funded by the Ministry of Land, Infrastructure and Transport (Grant RS-2023-00238018), and by the National Research Foundation of Korea (NRF) grant funded by the Korean government (MSIT) (No. NRF-2021M3H4A1A02048529). And we are also very grateful for the support from DGIST Supercomputing Bigdata Center.

Appendix A. Supplementary data

Supplementary data to this article can be found online at https://doi.org/10.1016/j.etran.2024.100370.

Data availability

Data will be made available on request.

References

[1] Tepe B, Jablonski S, Hesse H, Jossen A. Lithium-ion battery utilization in various modes of e-transportation. ETransportation 2023;18. https://doi.org/10.1016/j.etran.2023.100274.
[2] 2011 international conference on clean electrical power. IEEE; 2011.
[3] Ogasa M. Application of energy storage technologies for electric railway vehicles-examples with hybrid electric railway vehicles. IEEJ Trans Electr Electron Eng 2010;5:304–11. https://doi.org/10.1002/tee.20534.
[4] Lyu P, Liu X, Qu J, Zhao J, Huo Y, Qu Z, Rao Z. Recent advances of thermal safety of lithium ion battery for energy storage. Energy Storage Mater 2020;31:195–220. https://doi.org/10.1016/j.ensm.2020.06.042.
[5] Liu K, Liu Y, Lin D, Pei A, Cui Y. Materials for lithium-ion battery safety. https://www.science.org; 2018.
[6] Xia G, Cao L, Bi G. A review on battery thermal management in electric vehicle application. J Power Sources 2017;367:90–105. https://doi.org/10.1016/j.jpowsour.2017.09.046.
[7] Ould Ely T, Kamzabek D, Chakraborty D. Batteries safety: recent progress and current challenges. Front Energy Res 2019;7. https://doi.org/10.3389/fenrg.2019.00071.
[8] Schöberl J, Ank M, Schreiber M, Wassiliadis N, Lienkamp M. Thermal runaway propagation in automotive lithium-ion batteries with NMC-811 and LFP cathodes: safety requirements and impact on system integration. ETransportation 2024;19:100305. https://doi.org/10.14459/2023m.
[9] Peng R, Kong D, Ping P, Wang G, Gao X, Lv H, Zhao H, He X, Zhang Y, Dai X. Thermal runaway modeling of lithium-ion batteries at different scales: recent advances and perspectives. Energy Storage Mater 2024;69. https://doi.org/10.1016/j.ensm.2024.103417.
[10] Wang G, Ping P, Kong D, Peng R, He X, Zhang Y, Dai X, Wen J. Advances and challenges in thermal runaway modeling of lithium-ion batteries. Innovation 2024;5. https://doi.org/10.1016/j.xinn.2024.100624.
[11] Qin P, Sun J, Yang X, Wang Q. Battery thermal management system based on the forced-air convection: a review. ETransportation 2021;7. https://doi.org/10.1016/j.etran.2020.100097.
[12] Peng J, Zhao X, Ma J, Meng D, Zhu J, Zhang J, Yan S, Zhang K, Han Z. Enhancing lithium-ion battery monitoring: a critical review of diverse sensing approaches. ETransportation 2024;22. https://doi.org/10.1016/j.etran.2024.100360.
[13] Kang T, Lee PY, Kwon S, Yoo K, Kim J. Regional resistance-based spatial thermal model for checking non-uniformed temperature distribution and evolution of pouch type lithium-ion batteries. Appl Therm Eng 2021;192. https://doi.org/10.1016/j.applthermaleng.2021.116936.
[14] Jang DS, Yun S, Hong SH, Cho W, Kim Y. Performance characteristics of a novel heat pipe-assisted liquid cooling system for the thermal management of lithium-ion batteries. Energy Convers Manag 2022;251. https://doi.org/10.1016/j.enconman.2021.115001.
[15] Saechan P, Dhuchakallaya I. Numerical study on the air-cooled thermal management of Lithium-ion battery pack for electrical vehicles. Energy Rep 2022;8:1264–70. https://doi.org/10.1016/j.egyr.2021.11.089.
[16] Akbarzadeh M, Jaguemont J, Kalogiannis T, Karimi D, He J, Jin L, Xie P, Van Mierlo J, Berecibar M. A novel liquid cooling plate concept for thermal management of lithium-ion batteries in electric vehicles. Energy Convers Manag 2021;231. https://doi.org/10.1016/j.enconman.2021.113862.
[17] Sheng L, Su L, Zhang H, Li K, Fang Y, Ye W, Fang Y. Numerical investigation on a lithium ion battery thermal management utilizing a serpentine-channel liquid cooling plate exchanger. Int J Heat Mass Tran 2019;141:658–68. https://doi.org/10.1016/j.ijheatmasstransfer.2019.07.033.
[18] Wang G, Kong D, Ping P, Wen J, He X, Zhao H, He X, Peng R, Zhang Y, Dai X. Revealing particle venting of lithium-ion batteries during thermal runaway: a

multi-scale model toward multiphase process. ETransportation 2023;16. https://doi.org/10.1016/j.etran.2023.100237.
[19] Xu J, Guo Z, Xu Z, Zhou X, Mei X. A systematic review and comparison of liquid-based cooling system for lithium-ion batteries. ETransportation 2023;17. https://doi.org/10.1016/j.etran.2023.100242.
[20] Calearo L, Thingvad A, Ziras C, Marinelli M. A methodology to model and validate electro-thermal-aging dynamics of electric vehicle battery packs. J Energy Storage 2022;55. https://doi.org/10.1016/j.est.2022.105538.
[21] Xu Z, Zhang C, Sun B, Liu SZ. The electric-thermal coupling simulation and state estimation of lithium-ion battery. J Energy Storage 2023;58. https://doi.org/10.1016/j.est.2022.106431.
[22] He J, Sazzad Hosen M, Youssef R, Kalogiannis T, Van Mierlo J, Berecibar M. A lumped electro-thermal model for a battery module with a novel hybrid cooling system. Appl Therm Eng 2023;221. https://doi.org/10.1016/j.applthermaleng.2022.119874.
[23] Saqli K, Bouchareb H, M'sirdi NK, Oudghiri Bentaie M. Lithium-ion battery electro-thermal modelling and internal states co-estimation for electric vehicles. J Energy Storage 2023;63. https://doi.org/10.1016/j.est.2023.107072.
[24] Li Y, Zhou Z, Wu WT. Three-dimensional thermal modeling of Li-ion battery cell and 50 V Li-ion battery pack cooled by mini-channel cold plate. Appl Therm Eng 2019;147:829–40. https://doi.org/10.1016/j.applthermaleng.2018.11.009.
[25] Hua X, Heckel C, Modrow N, Zhang C, Hales A, Holloway J, Jnawali A, Li S, Yu Y, Loveridge M, Shearing P, Patel Y, Marinescu M, Tao L, Offer G. The prismatic surface cell cooling coefficient: a novel cell design optimisation tool & thermal parameterization method for a 3D discretised electro-thermal equivalent-circuit model. ETransportation 2021;7. https://doi.org/10.1016/j.etran.2020.100099.
[26] Chen Z, Qin Y, Dong Z, Zheng J, Liu Y. Numerical study on the heat generation and thermal control of lithium-ion battery. Appl Therm Eng 2023;221. https://doi.org/10.1016/j.applthermaleng.2022.119852.
[27] Tahir MW, Merten C. Multi-scale thermal modeling, experimental validation, and thermal characterization of a high-power lithium-ion cell for automobile application. Energy Convers Manag 2022;258. https://doi.org/10.1016/j.enconman.2022.115490.
[28] Jiang Y, Zhang L, Offer G, Wang H. A user-friendly lithium battery simulator based on open-source CFD. Digit Chem Eng 2022;5. https://doi.org/10.1016/j.dche.2022.100055.
[29] Kim S, Song J, Lee H, Jung S, Park J, Lee H, Lee YM. Simulation study on internal short circuits in a Li-ion battery depending on the sizes, quantities, and locations of Li dendrites. Front Mater 2022;9. https://doi.org/10.3389/fmats.2022.850610.
[30] Song J, Lee H, Kim S, Kang D, Jung S, Lee H, Kwon TS, Lee YM. A thermo-electrochemical model of 18.5V/50Ah battery module for railway vehicles. Front Mater 2022;9. https://doi.org/10.3389/fmats.2022.824168.
[31] Li H, Saini A, Liu C, Yang J, Wang Y, Yang T, Pan C, Chen L, Jiang H. Electrochemical and thermal characteristics of prismatic lithium-ion battery based on a three-dimensional electrochemical-thermal coupled model. J Energy Storage 2021;42. https://doi.org/10.1016/j.est.2021.102976.
[32] Hosseinzadeh E, Genieser R, Worwood D, Barai A, Marco J, Jennings P. A systematic approach for electrochemical-thermal modelling of a large format lithium-ion battery for electric vehicle application. J Power Sources 2018;382:77–94. https://doi.org/10.1016/j.jpowsour.2018.02.027.
[33] Ortiz Y, Arévalo P, Peña D, Jurado F. Recent advances in thermal management strategies for lithium-ion batteries: a comprehensive review. Batter 2024;10. https://doi.org/10.3390/batteries10030083.
[34] Sarkar S, Amin MT, El-Halwagi MM, Khan F. Thermal behavior of LiFePO4 battery at faster C-rates and lower ambient temperatures. Process Saf Environ Protect 2024;186:118–33. https://doi.org/10.1016/j.psep.2024.03.095.
[35] Saxon A, Yang C, Santhanagopalan S, Keyser M, Colclasure A. Li-ion battery thermal characterization for thermal management design. Batter 2024;10. https://doi.org/10.3390/batteries10040136.
[36] Morganti MV, Longo S, Tirovic M, Blaise CY, Forostovsky G. Multi-scale, electro-thermal model of NMC battery cell. IEEE Trans Veh Technol 2019;68:10594–606. https://doi.org/10.1109/TVT.2019.2943052.
[37] C.Y. Wang, V. Srinivasan, Computational battery dynamics (CBD)-electrochemical/thermal coupled modeling and multi-scale modeling, n.d.
[38] Katrašnik T, Mele I, Zelič K. Multi-scale modelling of Lithium-ion batteries: from transport phenomena to the outbreak of thermal runaway. Energy Convers Manag 2021;236. https://doi.org/10.1016/j.enconman.2021.114036.
[39] Gupta P, Gudmundson P. A multi-scale model for simulation of electrochemically induced stresses on scales of active particles, electrode layers, and battery level in lithium-ion batteries. J Power Sources 2021;511. https://doi.org/10.1016/j.jpowsour.2021.230465.
[40] Shi S, Gao J, Liu Y, Zhao Y, Wu Q, Ju W, Ouyang C, Xiao R. Multi-scale computation methods: their applications in lithium-ion battery research and development. Chin Phys B 2015;25. https://doi.org/10.1088/1674-1056/25/1/018212.
[41] Wu Q, Yang L, Li N, Chen Y, Wang Q, Song WL, Feng X, Wei Y, Sen Chen H. In-situ thermography revealing the evolution of internal short circuit of lithium-ion batteries. J Power Sources 2022;540. https://doi.org/10.1016/j.jpowsour.2022.231602.
[42] Grabow J, Klink J, Benger R, Hauer I, Beck HP. Particle contamination in commercial lithium-ion cells—risk assessment with focus on internal short circuits and replication by currently discussed trigger methods. Batter 2023;9. https://doi.org/10.3390/batteries9010009.
[43] Liu X, Zhang L, Yu H, Wang J, Li J, Yang K, Zhao Y, Wang H, Wu B, Brandon NP, Yang S. Bridging multiscale characterization technologies and digital modeling to evaluate lithium battery full lifecycle. Adv Energy Mater 2022;12. https://doi.org/10.1002/aenm.202200889.
[44] Naseri F, Gil S, Barbu C, Cetkin E, Yarimca G, Jensen AC, Larsen PG, Gomes C. Digital twin of electric vehicle battery systems: comprehensive review of the use cases, requirements, and platforms. Renew Sustain Energy Rev 2023;179. https://doi.org/10.1016/j.rser.2023.113280.
[45] Shi J, Zhang H, Yu H, Xu Y, Xu S, Sheng L, Feng X, Wang X. Experimental determinations of thermophysical parameters for lithium-ion batteries: a systematic review. ETransportation 2024;20. https://doi.org/10.1016/j.etran.2024.100321.
[46] E. Rasheed, B. Hussain Maula -, A general energy balance for battery systems you may also like advanced topics in computational partial differential equations: numerical methods and diffpack programming T D katsaounis-measurements of the natural radioactivity from Baghdad city soils using NaI (TI)detector, n.d.
[47] Wei L, Lu Z, Cao F, Zhang L, Yang X, Yu X, Jin L. A comprehensive study on thermal conductivity of the lithium-ion battery. Int J Energy Res 2020;44:9466–78. https://doi.org/10.1002/er.5016.
[48] Xie Y, Fan Y, Yang R, Zhang K, Chen B, Panchal S, Zhang Y. Influence of uncertainty of thermal conductivity on prediction accuracy of thermal model of lithium-ion battery. IEEE Trans Transport Electrification 2024. https://doi.org/10.1109/TTE.2024.3352663.